

Manuscript Number: ADES-D-14-00699R2

Title: Topology optimization of compliant mechanisms using element-free Galerkin method

Article Type: Research Paper

Keywords: Topology optimization; Compliant mechanisms; Shepard function; Meshless method, Geometrical non-linearity.

Corresponding Author: Dr. Zhen Luo, Ph.D.

Corresponding Author's Institution: University of Technology, Sydney

First Author: Yu Wang

Order of Authors: Yu Wang; Zhen Luo, Ph.D.; Jinglai Wu, Ph.D.; Nong Zhang, Ph.D.

Abstract: This paper will propose a topology optimization approach for the design of large displacement compliant mechanisms with geometrical non-linearity by using the element-free Galerkin (EFG) method. In this method, the Shepard function is applied to construct a physically meaningful density approximant, to account for its non-negative and range-bounded property. Firstly, in terms of the original nodal density field, the Shepard function method functionally similar to a density filter is used to generate a non-local nodal density field with enriched smoothness over the design domain. The density of any node can be evaluated according to the nodal density variables located inside the influence domain of the interested node. Secondly, in the numerical implementation the Shepard function method is again employed to construct a point-wise density interpolant. Gauss quadrature is used to calculate the integration of background cells numerically, and the artificial densities over all Gauss points can be determined by the surrounding nodal densities within the influence domain of the concerned computational point. Finally, the moving least squares (MLS) method is applied to construct the shape functions using the weight functions with compact support for assembling the meshless approximations of state equations. Since MLS shape functions are lack of the Kronecker delta function property, the penalty method is applied to enforce the essential boundary conditions. A typical large-deformation compliant mechanism is used as the numerical example to demonstrate the effectiveness of the proposed method.

Response to Reviewers' Comments

Manuscript: ADES-D-14-00699

Title: Topology Optimization for Micro Compliant Mechanisms using the Element-free Galerkin Method

Authors: Yu Wang, Zhen Luo, Jinglai Wu, Nong Zhang

Dear Editors,

Thanks for your efforts, as well as the reviewer's comments in further improving this manuscript. We have tried to answer the reviewer's questions and incorporated the changes into the 2nd revised submission. In the following, we will address the main questions raised by the reviewer, item by item. It is noted that all changes have been highlighted in the manuscript with yellow Highlight color.

Thank you once more,

Regards,

Zhen

Replies to Reviewer's Comments

Reviewer's comment 1.1: The authors have cited the paper by He et al. (Ref. [23]). However, the authors did not properly discuss the method and results in the paper. For instance, [23] also did optimization of compliant mechanisms considering nonlinearity (see their Numerical Example 3), which should be mentioned in the end of Paragraph 6, Introduction.

Authors' reply: *Thanks. By following the reviewer's suggestion, we have commented and cited this paper in the 2nd revised submission.*

Reviewer's comment 1.2: Most of incorrect English grams and spellings have been corrected, unless some followings,

- (i) Page 5, Line 16, "tried to applied" should be "tried to apply";
- (ii) Paragraph 6, Introduction, "the number of research works are " should be "the number ... is";
- (iii) Paragraph 6, Introduction, "Luo and et al." should be "Luo et al.";
- (iv) Page 6, Last line, "Final" should be "Finally";

Authors' reply: *They have been corrected in the revised version.*

Reviewer's comment 1.3: In the meshless method, the influence domain and the support domain are quite different concepts, which are used for interpolating/approximating points and nodes, respectively. They should also be distinguished in the present paper.

Authors' reply: *In this paper the influence domain is used for density interpolation, and the support domain is used to approximate the displacement field in MLS meshless approximations.*

Highlights

- 1: An alternative topology optimization method for the design of large displacement compliant mechanisms with geometrical nonlinearity;
- 2: Using the Shepard interpolation functionally as a density filter to enrich the smoothness of the density field over the meshless field node;
- 3: The Shepard function method is used again to interpolate the densities at all computational points to construct a physically meaningful material density field;
- 4: The moving least squares (MLS) method is applied to construct the shape functions for assembling the meshless approximations of state equations.

Submitted to *Advances in Engineering Software*

Original Submission: 06 Nov 2014, ADES-D-14-00699.

Revised Submission R1: 12 Jan 2015 ADES-D-14-00699 R1.

Topology optimization of compliant mechanisms using element-free Galerkin method

by

Yu Wang, Zhen Luo*, Jinglai Wu, Nong Zhang

School of Electrical, Mechanical and Mechatronic Systems

The University of Technology, Sydney, NSW 2007, Australia

* Correspondence author of the manuscript submission

(Dr Z. Luo, Email: zhen.luo@uts.edu.au; Phone: +61 2 9514 2994; Fax: +61 2 9514 2655)

*This paper is submitted for possible publication in **Advances in Engineering Software**. It has not been previously published, is not currently submitted for review to any other journals, and will not be submitted elsewhere during the peer review.*

Abstract

This paper will propose a topology optimization approach for the design of large displacement compliant mechanisms with geometrical non-linearity by using the element-free Galerkin (EFG) method. In this method, the Shepard function is applied to construct a physically meaningful density approximant, to account for its non-negative and range-bounded property. Firstly, in terms of the original nodal density field, the Shepard function method functionally similar to a density filter is used to generate a non-local nodal density field with enriched smoothness over the design domain. The density of any node can be evaluated according to the nodal density variables located inside the influence domain of the interested node. Secondly, in the numerical implementation the Shepard function method is again employed to construct a point-wise density interpolant. Gauss quadrature is used to calculate the integration of background cells numerically, and the artificial densities over all Gauss points can be determined by the surrounding nodal densities within the influence domain of the concerned computational point. Finally, the moving least squares (MLS) method is applied to construct the shape functions using the weight functions with compact support for assembling the meshless approximations of state equations. Since MLS shape functions are lack of the Kronecker delta function property, the penalty method is applied to enforce the essential boundary conditions. A typical large-deformation compliant mechanism is used as the numerical example to demonstrate the effectiveness of the proposed method.

Keywords: Topology optimization; Compliant mechanisms; Shepard function; Meshless method, Geometrical non-linearity.

1. Introduction

Topology optimization is a numerical approach to determine the best distribution of material within a design space under specific loads and boundary conditions, so that the resulting layout can meet a prescribed set of performance targets. In the past two decades, as a lately developed approach in structural optimization, topology optimization has experienced considerable development with many applications in a wide range of engineering disciplines [11]. By now, various schemes have been developed for topology optimization of structures, such as the homogenization method [9,21], the solid isotropic material with penalization (SIMP) method [53,40,10], the evolutionary structural optimization (ESO) method [51], and the level set-based method [45,49,1,34], as well as some improved methods, e.g. the pointwise-density interpolation (PDI) method [39,22,27,38]. Topology optimization methods have been applied to a variety of applications for structures, materials and mechanisms, e.g. the design of compliant mechanisms.

Unlike the conventional rigid-body mechanisms, which attain mobility from hinges, bearings and sliders, compliant mechanisms gain their mobility from relative flexibility of the constituents [24]. The synthesis of compliant mechanisms is mainly used to control the ratios between output and input displacements or forces, which can be described by geometrical advantage and/or the mechanical advantage. Compared to the rigid-body counterparts, compliant mechanisms can be built using fewer parts with less wear, friction, noise and backlash, and require less assembly processes. Due to these advantages, compliant mechanisms have been widely used in precision control devices and Micro Electro Mechanical Systems (MEMS).

To apply topology optimization in mechanical designs, it is applicable to use linear analysis to find structural responses under the assumption of small displacement. But for structures involving large displacement or large rotation effect, it is necessary to consider geometrical non-linear analysis in the process of topology optimization [15,14,18,43,35,23]. It is also known that many parameters of materials may be subject to non-linearity. However in the design of compliant mechanisms the geometrical non-linearity is more important than material non-linearity [43]. Hence, in regards to topology optimization

for practical compliant mechanisms, it is important to include geometrical non-linearity in the process of numerical analysis [47,48,43,35]. For instance, Sigmund [47,48] investigated topology optimization of multiphysics compliant actuators with large deformation for single material, and multi-material structures. Pedersen et al. [43] developed a topology optimization method for the design of large-displacement compliant mechanisms for path-generating. Luo and Tong [35] proposed a parameteric level set method for topological shape design of compliant mechanisms with geometrical non-linearity.

It is noted that the numerical process of most works for topology optimization of large deformation compliant mechanisms are often based on the standard finite element method (FEM) [43,47,48], which relies on meshes or elements that are connected together by meshes in a properly predefined manner. It is noted that the accuracy of numerical solution may be degraded seriously due to mesh distortion for the analysis of large deformation of compliant mechanisms. In this case, the standard FEM will experience difficulties in treating discontinuity caused by the inconsistency of mesh grids [8].

To overcome this limitation of the standard FEM, several alternative methods have been developed to perform numerical analysis for topology optimization problems, without having to keep the connectivity of structured elements. To this end, some researchers have tried to apply meshless methods to topology optimization problems, only in terms of a set of arbitrarily scattered field nodes rather than structured meshes. The meshless or meshfree methods are relatively simple but able to provide sufficient numerical accuracy yet stability for certain classes of problems [7,3,31]. The typical meshless methods include the smooth particle hydrodynamic method (SPH) [19], the reproducing kernel particle method (RKPM) [32], the hp-clouds (HP) method [17], the partition of unity method (PUM) [4], the element-free Galerkin (EFG) method [6], the meshless local Petrov-Galerkin (MLPG) method [2], and the point interpolation method (PIM) [30,20]. In particular, the EFG method [e.g. 6] with weak forms has received great popularity in a range of areas including topology optimization of structures, due to its good numerical stability and accuracy for problems of computational solids mechanics. In EFG methods, the MLS approximation is usually used to construct the meshless shape functions, and the Galerkin technique of

weak-forms is employed to discretise the state equation. This method is “meshless” in terms of the interpolation of design variables. However, the background cells independent of field nodes are required to integrate a weak form over the problem domain. Furthermore, the MLS approximation is required to be enforced to satisfy the Kronecker delta function property. One attractive feature of MLS methods is that its continuity can be inherited from the continuity of the selected weight function.

The meshless methods have been applied to topology optimization problems to simulate the large deformation effect of structures [15,29,16,23]. However, having respect to topology optimization of large displacement compliant mechanisms, the number of research works is relatively small. For example, Du *et al.* [16] applied the EFG method to implement the geometrical nonlinear thermo-mechanical compliant mechanisms and showed that the meshless method can overcome the convergent difficulty in standard FEM. Luo *et al.* [36] introduced the meshless Galerkin method into the level set approach to develop a topological optimization method, which is further applied to multiphysics compliant actuators involving large deformation effect [37]. More recently, He *et al.* [23] applied PIM [30,20] to topology optimization problems for the design of structures and compliant mechanisms involving geometrical nonlinearity.

Since the meshless method is more capable of modelling the large displacement effect of the geometrical non-linearity [15,18,43], this paper attempts to propose a meshless topology optimization method for micro complaint mechanisms based on the EFG method. In this method, the point-wise densities which are considered as design variables are uniformly described based on a set of scattered field nodes inside the design domain. Firstly, in terms of the original set of meshless density field, the Shepard function method functioned as a density filter is applied to generate a non-local nodal density field with enriched smoothness over the design domain. Secondly, instead of using the MLS approximants to formulate both the shape function and approximate densities over the computational points, the Shepard function method is also employed to approximate the densities on the computational points, while MLS approximants is used to formulate the trial function. Since the Shepard function method possesses non-negative and range-bounded property, it can ensure a physically meaningful approximation of topology optimization design.

Finally, the MLS-shape function together with the Galerkin global weak-form is applied to develop the meshless approximation for the displacement field. Since the shape function using the MLS approximants does not satisfy the Kronecker Delta criterion [6,7], a penalty method is used to enforce the essential boundary conditions. To simulate large-displacements of compliant mechanisms, the output displacement maximization has been used as an objective function in this study.

2. Nodal Density-based Approximation Scheme

Shepard function method is a method for multivariate interpolations of scattered data, which can assign values to unknown points by using values from the scattered set of known points. In this study, the Shepard function is employed to construct a non-local pointwise density-based approximant, based on the concept of elemental SIMP [11]. SIMP has received much popularity due to its implementation easiness and conceptual simplicity, which has been widely used to relax the discrete topology optimization problem by allowing the design variables taking intermediate densities from 0 and 1.

The Shepard function satisfies the zero order completeness for representing constant function and possesses the properties of non-negative and range-bounded, which are the fundamental requirements for topology optimization. Thus, a family of Shepard function is firstly used as a non-local approximant to construct a density field with global smoothness over the design space. Secondly, it is applied to interpolate the point-wise densities of computational points inside the design domain.

2.1 Shepard function

Let $\varphi_i (i=1,2,\dots,n_H)$ denote a set of non-negative data values at the associated sampling points $x_i=(X_i,Y_i)$ within the support radius r of an arbitrary point x . (X_i,Y_i) defines the i th point location in the given Cartesian coordinate system. The approximation of the Shepard function method is stated as

$$\varphi(x) = \sum_{i=1}^{n_H} \Theta_i(x) \varphi_i \quad (1)$$

where n_H is the number of the nodes within the influence domain of current point x . The Shepard

function $\Theta_i(x)$ is expressed as a normalized formulation, which is given by

$$\Theta_i(x) = \frac{\omega_i(x-x_i)}{\sum_{j=1}^{n_H} \omega_j(x-x_j)} \quad (2)$$

where $\omega_i(x-x_i)$ is the weight function, which is zero outside the domain of influential support, and decays with the distance from the interest point. In this study, when the Shepard function is used as the nodal density approximant [28,26,27], the weight function can be chosen as

$$\omega_i(x-x_i) = \frac{3}{\pi r^2} \max\left(0, 1 - \frac{D_i(x)}{r}\right) \quad (3)$$

where $D_i(x) = x - x_i = \sqrt{(X - X_i)^2 + (Y - Y_i)^2}$. It is noted that the Shepard function $\Theta_i(x)$ possesses the following properties: (1) $\sum_{i=1}^{n_H} \Theta_i(x) = 1$; (2) $1 \geq \Theta_i(x) > 0$.

2.2 Non-local Nodal Density Approximation using Shepard function

It is apparent that the Shepard function has a mechanism similar to the smoothing effect of the density filtering schemes [12,33]. Meanwhile, the approximated values via the Shepard function are bounded between lower and upper values of the sampling points. This is the essential property for ensuring a physically meaningful density field approximant in topology optimization. The Shepard function is originally defined as a global interpolation. To improve its computational efficiency while maintain a reasonable accuracy, this study approximates the density at any field node in terms of the density variables of those field nodes located within a compact influence domain “r”, as shown in Fig. 1(a).

With the Shepard function method, any density variable for a meshless field node can be calculated as

$$\bar{\rho}(x) = \sum_{i=1}^{n_H} \Theta_i(x) \rho_i \quad (4)$$

where the nodal density variable $\bar{\rho}(x)$ can be obtained by searching the total number of surrounding nodal variables ρ_i within the influence domain of the node x , and $\bar{\rho}(x)$ is density at the concerned field node to be approximated by the Shepard function. n_H is the number of nodes within the influence domain.

This weight function is a radially linear ‘hat’ function defined by [12]. It means that only nearby points are considered in computing any approximated value. It is straightforward that the Shepard function can meet the following necessary conditions to ensure a physically meaningful density approximant in topology optimization of continuum structures: (1) $0 \leq \bar{\rho}(x) \leq 1$; (2) $\partial \bar{\rho}(x) / \partial \rho_i \geq 0$.

With the density field approximant, the Young’s modulus at the meshless field node x can be defined by

$$E(x) = \bar{\rho}^p(x) E_0 = \left(\sum_{i=1}^{n_H} \Theta_i(x) \rho_i \right)^p E_0 \quad (5)$$

where E_0 represents the full-solid state material property. The design variable ρ_i acts as the intrinsic nodal density allowing intermediate values between 0 and 1. The influence domain of the density interpolation is used to identify the design variable points influencing the density value of each computational point. It has been shown by [26] that the influence domain size used in the Shepard function-based density interpolation has a certain length-scale control effect. It is suggested that values between 1 to 3 times of the average distance can provide meaningful solutions, and 1.5 times of the average density point distance is an appropriate value for the radius of circular influence domain.

2.3 Point-wise Density Interpolation using Shepard function

Secondly, the Shepard function is utilized to construct an interpolation scheme for evaluating point-wise densities over all computational points inside the design domain, according to the previously obtained and smoothed densities of meshless field nodes. For implementing Gauss quadrature of the system stiffness matrix, the background virtual cells are required, which are independent of the set of field nodes. Here, 4×4 Gauss quadrature is used to numerically calculate the uniform integration cells according to the location of the computational points. The densities on the computational points (Gauss points) are interpolated via the Shepard function method, which can be given as

$$\bar{\rho}_{gp} = \sum_{i=1}^{n_s} \theta_i(x_{gp}) \bar{\rho}(x) = \sum_{i=1}^{n_s} \left(\frac{\omega_i(x)}{\sum_{j=1}^{n_s} \omega_j(x)} \right) \bar{\rho}(x) \quad (6)$$

where $x_{gp}=(X_{gp},Y_{gp})$, and (X_{gp},Y_{gp}) defines the location of Gauss point in the given Cartesian coordinate system. To let the Shepard function $\theta_i(x)$ satisfy the interpolation condition $\theta_i(x_j)=\delta_{ij}$, where $i,j=1,2,\dots,n_s$, a point-wise density field over the computational points can be constructed via the interpolation of the Shepard function with the following weight functions, expressed as

$$\omega_i(x) = \omega(D) = \begin{cases} \frac{2}{3} - 4D^2 + 4D^3 & D \leq 1/2 \\ \frac{4}{3} - 4D + 4D^2 - \frac{4D^3}{3} & 1/2 < D \leq 1 \\ 0 & D > 1 \end{cases} \quad (7)$$

where $D = x_{gp} - x = \frac{\sqrt{(X_{gp} - X)^2 + (Y_{gp} - Y)^2}}{r}$

As indicated in Fig. 1(b), “r” is radius of influence domain, and there are eight nodes which are considered as the associated points to the concerned computational point. It is easy to see that the Shepard function here satisfies the following properties:

- (1) Non-negative and range-bounded $0 \leq \theta_i(x) \leq 1$;
- (2) Partition of unity $\sum \theta_i(x) = 1$;
- (3) Interpolation condition $\theta_i(x_j) = \delta_{ij}$.

In this way, the Shepard method can ensure a physically meaningful interpolation to generate a point-wise density field for the numerical implementation of the SIMP-based topology optimization. By applying the Shepard function method in approximating the densities on field nodes and interpolating the densities on computational points, the point-wise density approximant is finally expressed as

$$\bar{\rho}_{gp} = \sum_{j=1}^{n_s} \left\{ \theta_j(x_{gp}) \left(\sum_{i=1}^{n_H} \theta_i(x) \rho_i \right) \right\} \quad (8)$$

Using the background cells are required to implement Gauss quadrature of the system stiffness matrix, the system stiffness matrix can be expressed as

$$\mathbf{K} = \int_{\Omega} \mathbf{B}^T \mathbf{D}(x) \mathbf{B} dx \quad (9)$$

where \mathbf{B} is the geometric strain-displacement matrix, and \mathbf{D} is the elasticity constant matrix. Here, 4×4 Gauss quadrature is used to numerically calculate the uniform integration cells according to the location of the computational points.

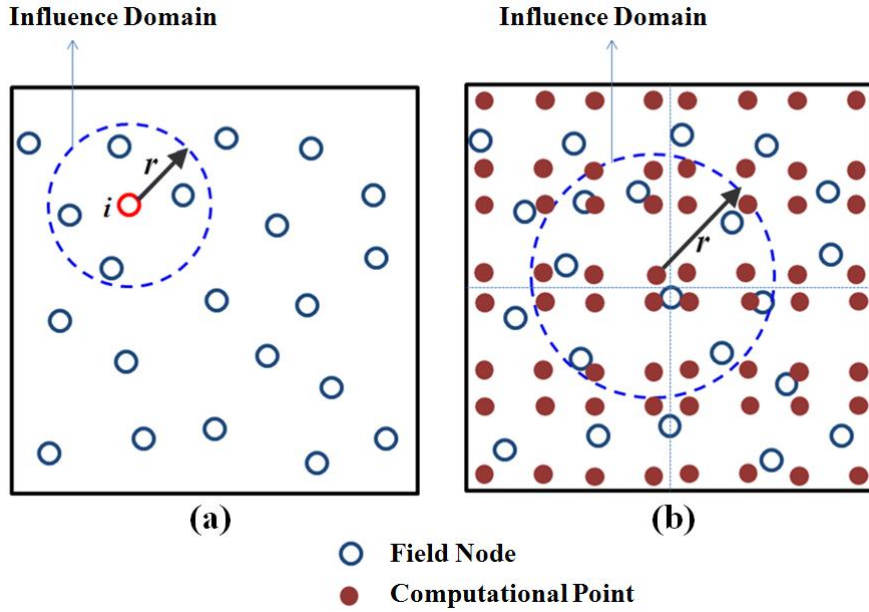


Figure 1(a). Influence domain of nodal design variable; (b). Influence domain of computational point

Using the 4×4 Gauss numerical integration, the system stiffness matrix \mathbf{K} can be explicitly expressed by

$$\mathbf{K} = \sum_{i=1}^4 \sum_{j=1}^4 \left[\mathbf{h} \mathbf{B}^T(\xi_i, \eta_j) \mathbf{D}(\xi_i, \eta_j) \mathbf{B}(\xi_i, \eta_j) \left| \mathbf{J}(\xi_i, \eta_j) \right| w_i w_j \right] \quad (10)$$

where $\mathbf{D}(\xi_i, \eta_j)$ is the material elastic constants at each Gauss point, w is the corresponding weighting factors and h is the thickness of material. The elasticity constant $\mathbf{D}(\xi_i, \eta_j)$ can be expressed as follows:

$$\mathbf{D}(\xi_i, \eta_j) = \rho(\xi_i, \eta_j) \mathbf{D}_0 = \sum_{j=1}^{n_s} \left\{ \theta_j(\mathbf{x}_{gp}) \left(\sum_{i=1}^{n_H} \Theta_i(\mathbf{x}) \rho_i \right) \right\} \mathbf{D}_0 \quad (11)$$

where \mathbf{D}_0 is the material elastic tensor of the full-solid state material. Thus, the stiffness matrix of the finite element can be explicitly given by

$$\mathbf{K} = \sum_{i=1}^4 \sum_{j=1}^4 \left[\mathbf{h} \mathbf{B}^T(\xi_i, \eta_j) \left(\sum_{j=1}^{n_s} \left\{ \theta_j(x_{gp}) \left(\sum_{i=1}^{n_H} \Theta_i(x) \rho_i \right) \right\} \mathbf{D}_0 \right) \mathbf{B}(\xi_i, \eta_j) \mathbf{J}(\xi_i, \eta_j) \mathbf{w}_i \mathbf{w}_j \right] \quad (12)$$

where N_n is the standard Lagrangian shape function, and n_e is the number of nodes in each element and equals to 4 here. x_n is the coordinates of n th node in each element.

3. Meshless Approximations using MLS Shape Function

The moving least squares (MLS) technique is used to construct the meshless approximations, and the MLS approximation for a general function $u(x)$ at x can be described as below [6,7]:

$$u^h(x) = \sum_{j=1}^m p_j(x) a_j(x) = \mathbf{p}^T(x) \mathbf{a}(x) \quad (13)$$

where $\mathbf{p}(x)$ is a complete polynomial of order m acting as the basis at x , and $\mathbf{a}(x)$ is the vector consisting of unknown coefficients. $a_j(x)$ ($j=1, \dots, m$) are the unknown parameters related to given points, which can be determined by minimizing a weighted discrete L_2 norm over all nodes in terms of the pre-known parameters u_l .

$$J = \sum_{l=1}^n \tilde{w}(x - x_l) \left(\sum_{j=1}^m p_j(x_l) a_j(x) - u_l \right)^2 \quad (14)$$

where n is the number of nodes within the local support of x . The weight function $\tilde{w}(x - x_l) \neq 0$. u_l is the nodal parameter of u at $x = x_l$. The minimization of J with respect to the coefficients $\mathbf{a}(x)$ results in a set of linear equations as

$$\frac{\partial J}{\partial a_j(x)} = 2 \sum_{l=1}^n \tilde{w}(x - x_l) \left(\sum_{j=1}^m p_j(x_l) a_j(x) - u_l \right) p_j(x_l) = 0 \quad (15)$$

The compact form for the above equation is given by

$$\mathbf{A}(x) \mathbf{a}(x) = \mathbf{B}(x) \mathbf{u} \quad (16)$$

Here \mathbf{u} is the vector consisting of the nodal parameters for all nodes inside the support domain, and $\mathbf{u}^T = [u_1, u_2, \dots, u_n]$. Solving Equation (16) for $\mathbf{a}(x)$ leads to

$$\mathbf{a}(x) = \mathbf{A}^{-1}(x) \mathbf{B}(x) \mathbf{u} \quad (17)$$

Substituting the above equation into Equation (13), we have the following the MLS approximant

$$u^h(x) = \sum_{I=1}^n \phi_I(x) u_I = \boldsymbol{\Phi}(x) \mathbf{u} \quad (18)$$

where $\boldsymbol{\Phi}(x)$ is the vector of MLS shape functions related to the n nodes in the local support domain of x .

The shape function $\phi_I(x)$ associated with node I at point x can be written as

$$\boldsymbol{\Phi}(x) = \mathbf{p}^T(x) (\mathbf{A}(x))^{-1} \mathbf{B}(x) \quad (19)$$

In this study, the cubic spline weight function with $C^2(\Omega)$ continuity is used, and the first-order derivative of the weight function, which is continuous over the entire domain, can be easily obtained via the chain rule of differentiation.

The weight function and its derivatives are written as a function of the normalized radius Υ as follows:

$$\tilde{w}(x - x_I) = w(\Upsilon) = \begin{cases} \frac{2}{3} - 4\Upsilon^2 + 4\Upsilon^3 & \text{for } \Upsilon \leq \frac{1}{2} \\ 0 & \text{for } \Upsilon > 1 \\ \frac{4}{3} - 4\Upsilon + 4\Upsilon^2 - \frac{4}{3}\Upsilon^3 & \text{for } \frac{1}{2} < \Upsilon \leq 1 \end{cases} \quad (20)$$

where $\Upsilon = \frac{d_I}{d_{ml}} = \frac{\|x - x_I\|}{d_{\max} c_I}$

here d_{ml} is the size of the support domain of the I^{th} node, which can be determined by d_{\max} and c_I . d_{\max} is a scaling parameter which is typically selected as 2.0-4.0 for a static analysis, and c_I is the distance to be decided by searching the surrounding nodes at the I^{th} node. It is noted that the support domains of a computational point for the calculation of displacement and the density interpolation are different. In this section, the support domain of the computational point is used to approximate the displacement field. In general, the computational accuracy of displacement field can be ensured by setting a reasonable value.

In MLS meshless approximations, each node is associated with a weight function of compact support, which is required to be non-zero only inside the domain of influence of node I , in order to generate a set of sparse discrete equations. A lower order polynomial basis can be used to generate higher continuous

approximations by choosing a proper weight function. Thus, the weight function plays an important role in meshless approximations. The MLS shape functions $N_i(x)$ have the following properties [7,3]:

(1) Order of the basis function is closely related to the consistency for completeness and reproducibility. Order $m=1$ (linear basis) can lead to linear consistency, which refers to the widely studied MLS shape function for meshless approximations, termed as “MLS-Shape function”.

(2) Considering the lowest order $m=0$ (constant basis), the MLS shape function will degenerate to the “Shepard function”, which owns non-negative and bound-ranged properties, like the method used to interpolate the densities on computational points.

(3) Partitions of unity, because the constant term is included in the basis.

(4) Desirable continuity of the approximation inherits from its weigh function of high continuity.

4. Geometrically nonlinear analysis using the EFG method

It is important to consider geometrical nonlinearity in compliant mechanism design, which assumes the compliant mechanism undergoes large displacement but the material behaviours remain linear. Using the principle of virtual displacement, the equilibrium equation about the nonlinear problem is expressed as

$$\Pi(\mathbf{u}) = \int_{\Omega} \bar{\mathbf{f}} \delta \mathbf{u} d\Omega + \int_{\Gamma_i} \bar{\mathbf{t}} \delta \mathbf{u} d\Gamma + \int_{\Omega} \mathbf{S} \delta \boldsymbol{\varepsilon} d\Omega = 0 \quad (21)$$

where \mathbf{S} is the second Piola-Kirchhoff stress matrix, \mathbf{u} is the displacement vector, $\boldsymbol{\varepsilon}$ is the Green Lagrangian strain vector. $\bar{\mathbf{f}}$ is the body force in design domain Ω , and $\bar{\mathbf{t}}$ is the force enforced on the natural boundary. The residual defined as the error using EFG method is then obtained as follows:

$$\mathbf{R}(\mathbf{u}) = \int_{\Omega} \boldsymbol{\Phi}^T \bar{\mathbf{f}} d\Omega + \int_{\Gamma} \boldsymbol{\Phi}^T \bar{\mathbf{t}} d\Gamma - \int_{\Omega} \mathbf{B}^T \mathbf{S} d\Omega = 0 \quad (22)$$

where \mathbf{B} is the matrix that transforms a change in displacement into a change in strain, which is a function of the nodal displacement \mathbf{u} . To solve the nonlinear equation, Eq. (21), the Newton-Raphson method [5] is used in this study. The relationship between $d\boldsymbol{\varphi}$ and $d\mathbf{u}$ is required to be determined.

$$d\mathbf{R}(\mathbf{u}) = \int_{\Omega} \mathbf{B}^T d\mathbf{S} d\Omega + \int_{\Omega} d\mathbf{B}^T \mathbf{S} d\Omega = \mathbf{K}_T d\mathbf{u} \quad (23)$$

where

$$d\mathbf{S} = \mathbf{D}d\mathbf{E} \quad (24)$$

$$\mathbf{E} = \mathbf{B}\mathbf{u} \quad (25)$$

Substituting Eq. (24) and (6) into the first integration of Eq. (23) will yield

$$\int_{\Omega} \mathbf{B}^T \mathbf{S} d\Omega = \left(\int_{\Omega} \mathbf{B}^T \mathbf{D} \mathbf{B} d\Omega \right) \mathbf{u} = \mathbf{K}_D \mathbf{u} \quad (26)$$

\mathbf{K}_D is the tangent stiffness related to the constitutive matrix, which is expressed as:

$$\mathbf{K}_D = \mathbf{K}_L + \mathbf{K}_N \quad (27)$$

where \mathbf{K}_L is the usual small displacement stiffness matrix as the one based on linear assumption, \mathbf{K}_N is the stiffness matrix caused by the geometrical non-linearity. They are stated as follows:

$$\mathbf{K}_L = \int_{\Omega} \mathbf{B}_L^T \mathbf{D} \mathbf{B}_L d\Omega \quad (28)$$

$$\mathbf{K}_N = \int_{\Omega} \left(\mathbf{B}_L^T \mathbf{D} \mathbf{B}_L + \mathbf{B}_N^T \mathbf{D} \mathbf{B}_N + \mathbf{B}_N^T \mathbf{D} \mathbf{B}_L \right) d\Omega \quad (29)$$

where

$$\mathbf{B}_L = \begin{bmatrix} \phi_{i,x} & 0 \\ 0 & \phi_{i,y} \\ \phi_{i,y} & \phi_{i,x} \end{bmatrix} \quad (30)$$

$$\mathbf{B}_N = \begin{bmatrix} L_{xx} \phi_{i,x} & L_{yx} \phi_{i,x} \\ L_{xy} \phi_{i,y} & L_{yy} \phi_{i,y} \\ L_{xx} \phi_{i,y} + L_{xy} \phi_{i,x} & L_{yx} \phi_{i,y} + L_{yy} \phi_{i,x} \end{bmatrix} \quad (31)$$

$$L_{xx} = \sum_{k=1}^n \phi_{k,x} u_x^k, \quad L_{yx} = \sum_{k=1}^n \phi_{k,x} u_y^k, \quad L_{xy} = \sum_{k=1}^n \phi_{k,y} u_x^k, \quad L_{yy} = \sum_{k=1}^n \phi_{k,y} u_y^k \quad (32)$$

In Eq. (30), (31) and (32), $\phi_{i,x}$ is the shape function derivative with respect to the coordinates of nodes, u_x^k is the displacement component of node k on the x axis.

The second integration in Eq. (23) can be expressed as

$$\int_{\Omega} d\mathbf{B}^T \mathbf{S} d\Omega = \left(\int_{\Omega} \mathbf{B}_{NL}^T \mathbf{S} \mathbf{B}_{NL} d\Omega \right) \mathbf{u} = \mathbf{K}_S \mathbf{u} \quad (33)$$

where

$$\mathbf{S} = \begin{bmatrix} S_{xx} & S_{xx} & 0 & 0 \\ S_{xx} & S_{xx} & 0 & 0 \\ 0 & 0 & S_{xx} & S_{xx} \\ 0 & 0 & S_{xx} & S_{xx} \end{bmatrix} \quad (34)$$

$$\mathbf{B}_{NL} = \begin{bmatrix} \phi_{i,x} & 0 \\ \phi_{i,y} & 0 \\ 0 & \phi_{i,x} \\ 0 & \phi_{i,y} \end{bmatrix} \quad (35)$$

\mathbf{K}_S is the initial stress matrix, which is a symmetric matrix dependent on the stress level. Thus, the tangent stiffness matrix \mathbf{K}_T can be expressed as

$$\mathbf{K}_T = \frac{d\mathbf{R}(\mathbf{u})}{d\mathbf{u}} = \mathbf{K}_L + \mathbf{K}_N + \mathbf{K}_S \quad (36)$$

To solve the non-linear equation, the Newton-Raphson iteration method [5] can be employed. Firstly, the initial value $\mathbf{u}^{(1)}$ is obtained via the linear equation:

$$\mathbf{K}_L \mathbf{u} - \mathbf{f} = 0 \quad (37)$$

where \mathbf{f} is the force vector.

Then, the displacement, strains and stresses, corresponding to the nodal parameter $\mathbf{u}^{(1)}$ are obtained. By substituting these values into Eq. (22), the residual $\varphi^{(1)}$ between the external and internal forces can be obtained. Thus, the increments of the nodal parameters are calculated as:

$$\Delta \mathbf{u} = -(\mathbf{K}_T)^{-1} \varphi^{(1)} \quad (38)$$

After that, we can figure out the new nodal parameter: $\mathbf{u}^{(2)} = \mathbf{u}^{(1)} + \Delta \mathbf{u}$. The above iteration is repeated until $\Delta \mathbf{u}$ satisfies the specified convergence criterion.

It is noted that the shape function formulated via the MLS method does not satisfy the Kronecker Delta condition $\phi_i(x_j) \neq \delta_{ij}$, which means the nodal parameter u_i is not equal to the value $u(x_i)$. Therefore, the imposition of essential boundary conditions is more complicated than that in the finite element method. In

this study, the essential boundary conditions are enforced using the penalty method. The essential boundary conditions can be accounted by means of a penalty formulation:

Find $u \in (H^i(\Omega))^3$, such that

$$\Pi_p = \frac{1}{2} \int_{\Omega} \boldsymbol{\varepsilon}^T \mathbf{D} \boldsymbol{\varepsilon} d\Omega - \int_{\Omega} \mathbf{u}^T \mathbf{b} d\Omega - \int_{\Gamma_t} \mathbf{u}^T \bar{\mathbf{t}} d\Gamma + \frac{\alpha}{2} \int_{\Gamma_u} (\mathbf{u} - \bar{\mathbf{u}})^T (\mathbf{u} - \bar{\mathbf{u}}) d\Gamma \quad (39)$$

is stationary, where $H^i(\Omega)$ is the Sobolev space of order i ; Π_p is the total potential energy; $\boldsymbol{\varepsilon}$ is the strain vectors; \mathbf{D} is the strain-stress matrix; Γ_t is the traction boundary; $\bar{\mathbf{t}}$ is prescribed traction; \mathbf{b} is a body force vector; the scalar α is a penalty parameter used to enforce the essential boundary conditions. $\bar{\mathbf{u}}$ are the prescribed nodal parameters on the boundary Γ_u .

Substituting Eq. (18) into Eq. (39) results in the following total potential energy, in matrix form, as

$$\Pi_p = \frac{1}{2} \mathbf{u}^T (\mathbf{K} + \mathbf{K}_u) \mathbf{u} - \mathbf{u}^T (\mathbf{f} + \mathbf{f}_u) \quad (40)$$

and invoking the stationary of Π_p obtains the following linear system:

$$(\mathbf{K} + \mathbf{K}_u) \mathbf{u} = \mathbf{f} + \mathbf{f}_u \quad (41)$$

where \mathbf{K} is the tangent stiffness matrix as in Eq. (27), and \mathbf{f} is the same as in Eq. (28). \mathbf{K}_u and \mathbf{f}_u are contributions from the essential boundary conditions, built from the following 2×2 matrices \mathbf{K}_{ij}^u and 2×1 matrices \mathbf{f}_i^u , respectively, as follows:

$$\mathbf{K}_{ij}^u = \alpha \int_{\Gamma_u} \phi_i \mathbf{S} \phi_j d\Gamma \quad (42)$$

and

$$\mathbf{f}_i^u = \alpha \int_{\Gamma_u} \phi_i \mathbf{S} \bar{\mathbf{u}} d\Gamma \quad (43)$$

and

$$\mathbf{S} = \begin{bmatrix} S_1 & 0 \\ 0 & S_2 \end{bmatrix} \quad (44)$$

$$S_1 = \begin{cases} 1 & \text{if } u_i \text{ is prescribed on } \Gamma_u, \\ 0 & \text{if } u_i \text{ is not prescribed on } \Gamma_u, \quad i = 1, 2 \end{cases} \quad (45)$$

An important consideration for using the penalty method is the choice of an appropriate penalty parameter α . From the experience, the penalty parameter can be chosen as $(10^3 \sim 10^7) \cdot E$, where E is the Young's modulus of the material under consideration. The penalty method presents the advantages, e.g. the dimension of the system is not increased and the matrix in the resulting system is symmetric and positive definite, provided that \mathbf{K} is symmetric and α is large enough.

5. Topology optimization of compliant mechanisms

5.1 Formulation of the optimization problem

Topology optimization of compliant mechanisms is to design a structure that converts an input to a desired output. In this study, the displacement inverter is considered as an example of compliant mechanisms. The displacement inverter is used to transfer work from the input port to the output port, and it must be possible to control the displacement amplification of the mechanism. The optimal design of the inverter is to maximize the displacement/force/work performed on a work piece modelled by a spring with stiffness. The stiffness value of the spring on output port can control the displacement amplification.

There are several different objective functions can be available for the design of compliant mechanisms. It is noted that most of them are originally for compliant mechanisms under the assumption of linear elasticity, which may not well suitable for the problem with geometrical non-linearity. It has shown that the displacement output can be used as the objective function to model the large displacement effect of them mechanism [43,35]. Thus, the optimization problem using meshless methods can be established as

$$\left\{ \begin{array}{l} \text{Maximize: } u_{out} \\ \text{Subject to: } \sum_{j=1}^n \rho_j V_j - \bar{V} = 0, \\ \rho_j^{min} \leq \rho_j \leq 1, (j = 1, 2, \dots, n) \\ \mathbf{a}(u, \delta u) = \mathbf{I}(\delta u), \quad u|_{\Gamma_D} = \bar{u}, \forall \delta u \in \mathbf{H}^1 \end{array} \right. \quad (46)$$

where

$$f(u, \delta u) = \frac{1}{2} \varepsilon_{ij}(u) D_{ijkl}(\rho(x)) \varepsilon_{kl}(\delta u) \quad (47)$$

As aforementioned, u is the displacement field, and δu is the virtual displacement field belonging to \mathbf{H}^1 . \bar{u} is the prescribed displacement on the admissible Dirichlet boundary Γ_D . ρ is design variable, which is the nodal density in this study. V_j is the discrete material volume and \bar{V} is the total material constrain. n is the number of the design variables in the space, and ρ_j^{min} is the lower bound of the design variables that is determined as 0.0001 to avoid the numerical singularity when computing the global stiffness matrix.

5.2 Design sensitivity analysis

To solve the optimization problem, it is necessary to compute the sensitivities (first-order derivatives) of the structural response with respect to the changes of the design variables, which can be determined by using the adjoint sensitivity analysis method. The output displacement can be expressed as

$$u_{out} = \mathbf{L}^T \mathbf{u} \quad (48)$$

where \mathbf{L} is a vector with the value 1 at the degree of the output point and with 0 at all other places. Introducing a vector of Lagrangian multipliers λ and assuming the equilibrium has been found by solving Eq. (22), nothing is changed by adding the term $\lambda^T \mathbf{R}$ to the objective function (48) as

$$u_{out} = \mathbf{L}^T \mathbf{u} + \lambda^T \mathbf{R}(\mathbf{u}) \quad (49)$$

Then sensitivity of the output displacement can be calculated as

$$\frac{du_{out}}{d\rho_i} = \mathbf{L}^T \frac{d\mathbf{u}}{d\rho_i} + \lambda^T \left(\frac{\partial \mathbf{R}}{\partial \mathbf{u}} \frac{d\mathbf{u}}{d\rho_i} + \frac{\partial \mathbf{R}}{\partial \rho_i} \right) \quad (50)$$

where

$$\frac{\partial \mathbf{R}}{\partial \mathbf{u}} = -\mathbf{K}_T$$

Since $\mathbf{R} = 0$ and the Lagrangian multiplier vector λ can be chosen freely, the unknown $\frac{d\mathbf{u}}{d\rho_i}$ in Eq. (50)

can be eliminated when λ is chosen such that

$$\left(\mathbf{L}^T - \lambda \mathbf{K}_T\right) \frac{d\mathbf{u}}{d\rho_i} = 0 \quad (51)$$

which can be obtained by solving the system of the following linear equation

$$\mathbf{K}_T \lambda = \mathbf{L} \quad (52)$$

By inserting λ into the Eq. (50), the sensitivity of the objective function can be simplified as

$$\frac{du_{out}}{d\rho_i} = \lambda^T \frac{\partial \mathbf{R}}{\partial \rho_i} \quad (53)$$

6. Numerical Example

The displacement inverter is used as a numerical example to show topology optimization process of the micro compliant mechanism design, as shown in Figure 2. The example is solved based on the proposed non-linear modelling of EFG method. The optimality criteria method is used to solve the optimization problem. To demonstrate the effectiveness of the proposed approach, the results will be compared with that obtained by using non-linear modelling of FEM and linear modelling of EFG method, respectively.

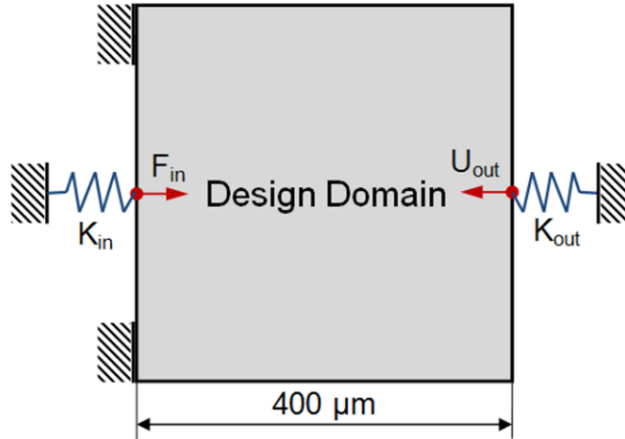


Figure 2. The displacement inverter design problem

As given in Figure 2, the design domain of displacement inverter is $400 \times 400 \mu\text{m}^2$. On the input port, the input work is modelled by a linear spring with stiffness K_{in} and a force F_{in} . The goal of the optimization problem is to maximize the displacement U_{out} , which is modelled by a spring with stiffness K_{out} . For simplicity of the computation, the design domain is discretised uniformly by using 41×41 nodes as shown in Figure 3, and 40×40 cells are used for integration, inside which the 4×4 Gauss points are used as the computational points (Figure 4). In this case, Yong's modulus is 3GPa, Poisson's Ratio is 0.3. An input

force $F_{in}=1\text{N}$, and an artificial spring with stiffness $K_{in}=5\times 10^4\text{N/m}$ are applied to the input port to simulate the input work. An artificial spring with stiffness $K_{out}=0.1\times 10^4\text{N/m}$ is used to simulate the resistance from a work piece. The material usage is limited to 25%.

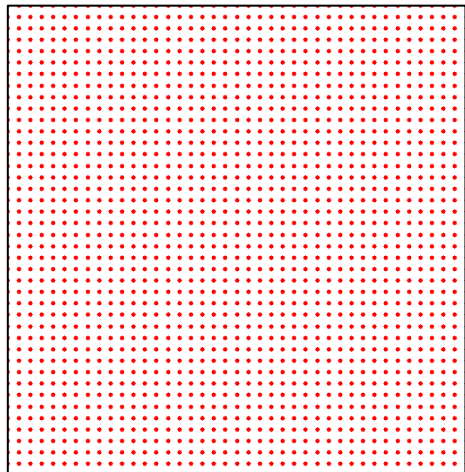


Figure 3. Design variables in design domain

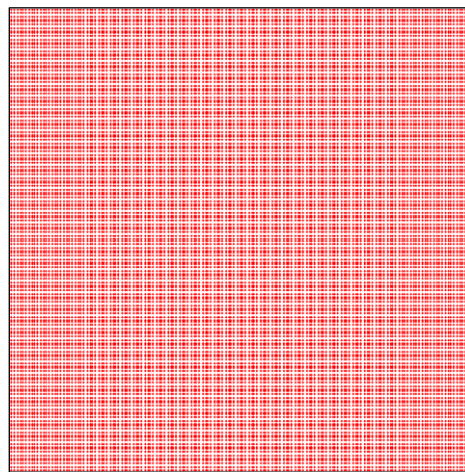
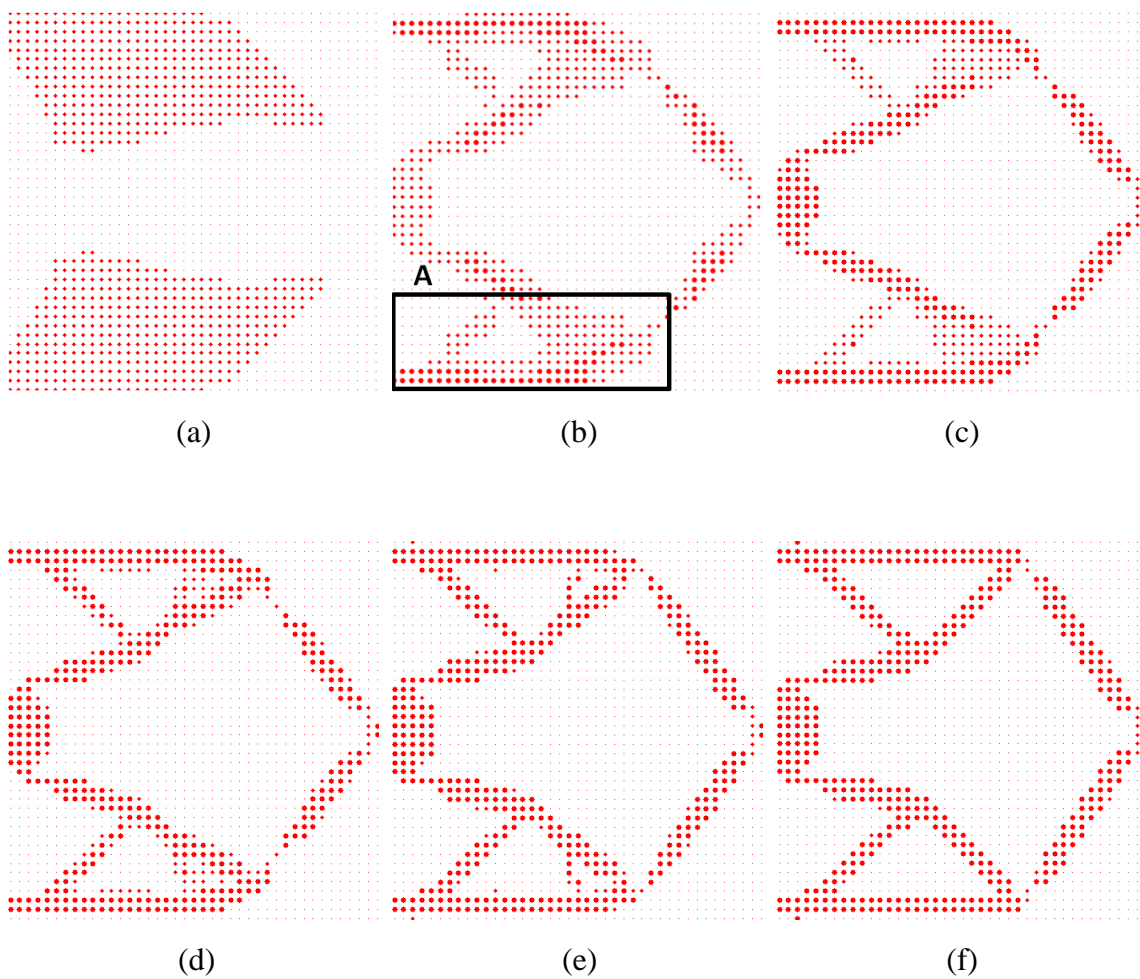


Figure 4. Computational points in design domain



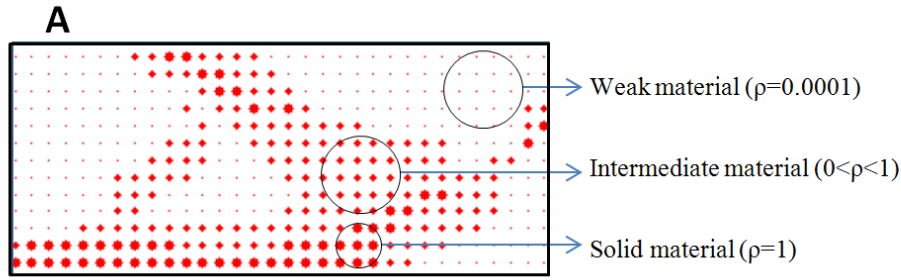


Figure 5. Topology plots of point-wise nodal densities: (a-e) intermediate results, and (f) optimal design.

As shown in Figure 5, a set of nodal densities acting as design variables of the topology optimization is used to represent material distribution which towards the lower limit 0.0001 (weak material phase) and the upper limit 1 (solid material phase) during the optimization. We can find that topology optimization is actually an iterative process to re-distribute a number of density points in the design space until these variables close to a so-called “0-1” distribution. It can be seen that the optimal topology does not have the discontinuously scattered nodes. It should be noted that the one-point connected hinges still appear in the optimal design, in order to enable the optimal structure have large rotation effect as a mechanism. However, the appearance of hinges is unfavourable in manufacturing. Furthermore, such a lumped compliant mechanism will easily subject to stress concentration and fatigue breakage [24]. For the issue of one-point connected hinges, it is out of the major scope of this paper. The reader may refer to some typical papers for more details [46,52].

Using the proposed EFG method, the displacement distortion plot related to the optimal design is shown in Figure 6. The output displacement of the optimal design is 37.06 μm . Figure 8 shows curves of the objective function and the volume constraint over the iterations. The evolution of the optimization process using the proposed EFG method is converged after 103 iterations. According to the curve of the volume constraint, the proposed method is mass conservative. We found that the optimal design obtained by the proposed non-linear modelling of EFG method is similar to those reported in [11]. The results in this case show that the proposed method can find the optimal design of large-displacement compliant mechanisms.

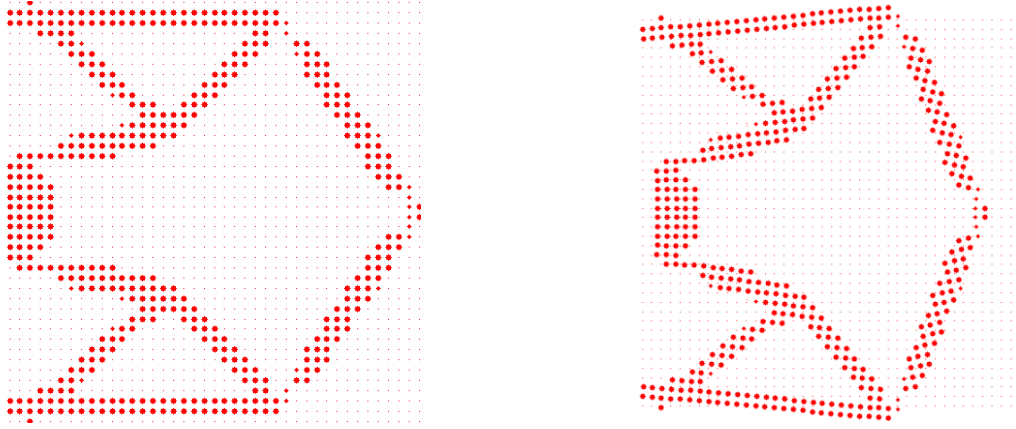


Figure 6. Topologies (left) and deformation (right) of optimized mechanism

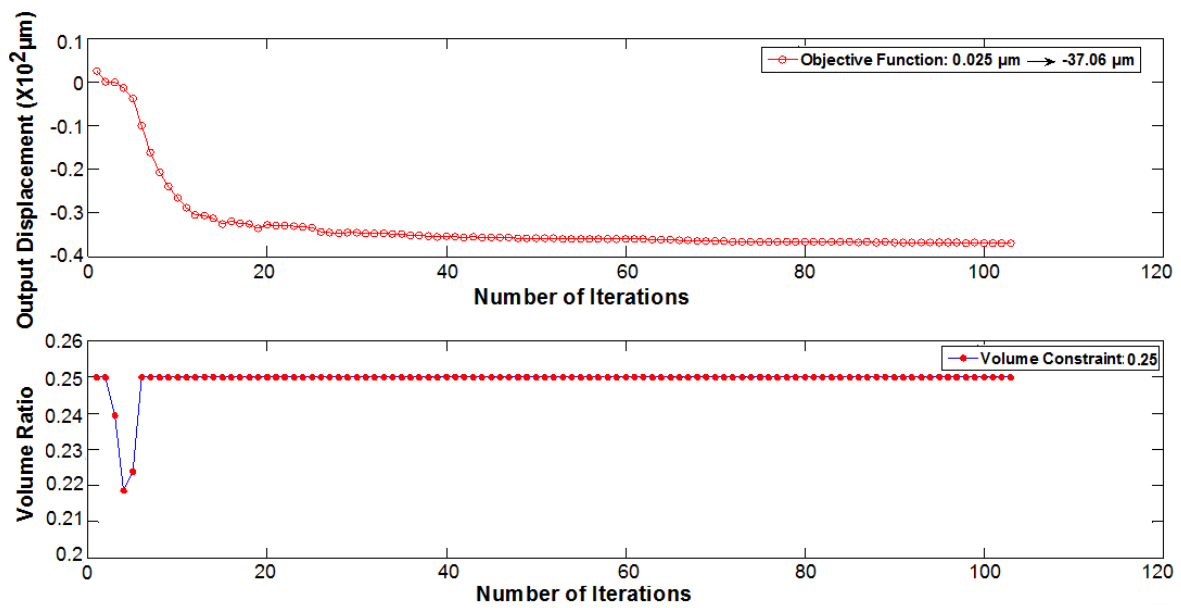


Figure 7. Iteration histories of objective function and volume constraint

To demonstrate the importance of non-linearity in the analysis of compliant mechanisms, the optimal topologies and deformations using non-linear modelling of EFG method, linear modelling of EFG method and non-linear modelling of FEM are compared under different input and output constraints. For the comparison with the FEM method, the design domain is discretised by 40×40 quad element in FEM approach while it is discretised by using 41×41 nodes uniformly scattered in the EFG approach. The parameters for the three cases are given in Table 1 and the optimal results are shown in Table 2.

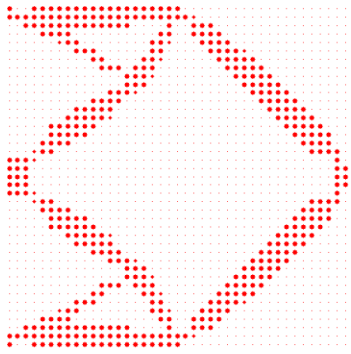
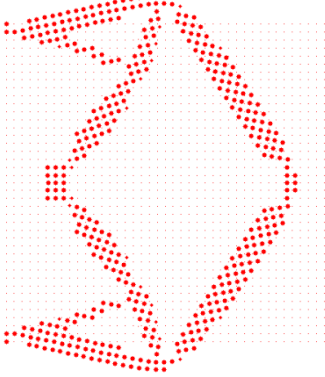
Compared with the FEM-based method, it can be seen that the EFG-based method is more capable to describe a distinct topology. This is caused by the difference of the design variables in these two methods.

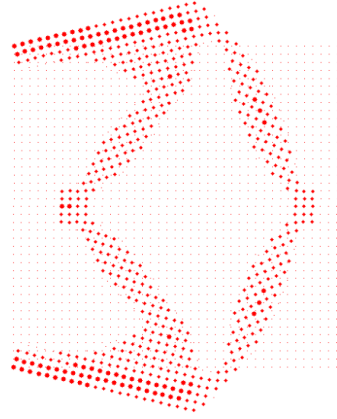
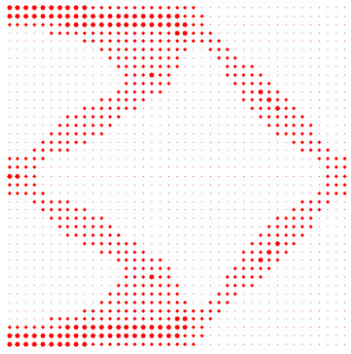
In the EFG method, the densities attached to the meshless field nodes are used as the design variables, while in FEM method the density of each finite element is assumed to be constant. Through comparing the topology obtained by using the linear and non-linear analysis of the EFG method, it can be seen that the displacement inverter with the linear EFG model has thinner connections and bars than that obtained by the non-linear EFG model. It's known the topologies with thinner hinges and bars make it possible for the mechanism to bend and implement larger displacement outputs. The main objective of displacement inverter is to maximize the displacement at the output port. According to the results obtained in Cases 1 and 2, the output displacement of the inverter by non-linear EFG model is larger than the linear EFG model and non-linear FEM model. The numerical results demonstrate that the non-linear modelling of EFG method is more suitable to capture the structural behaviour of large deformation.

Table 1. Initial parameters and corresponding optimal solutions for case 1-3

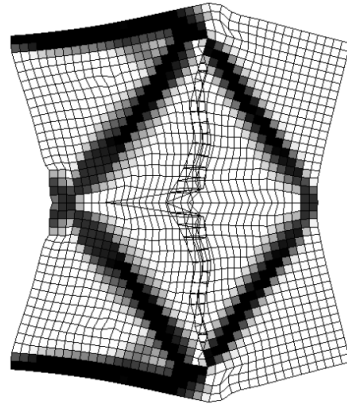
Case	F_{in}	K_{in}	K_{out}	U_{out} (by non-linear EFG)	U_{out} (by linear EFG)	U_{out} (by non-linear FEM)
1	1N	$1 \times 10^4 \text{N/m}$	$1 \times 10^4 \text{N/m}$	37 μm	32 μm	29.4 μm
2	0.5N	$1 \times 10^4 \text{N/m}$	$0.1 \times 10^4 \text{N/m}$	60.13 μm	56.1 μm ,	48.7 μm
3	1N	$1 \times 10^4 \text{N/m}$	$0.1 \times 10^4 \text{N/m}$	122.8 μm		

Table 2. Comparison of optimized topologies and deformation using different methods

Case	Optimized topology	Deformation of optimized mechanism
1		
Non-linear modelling using EFG method		

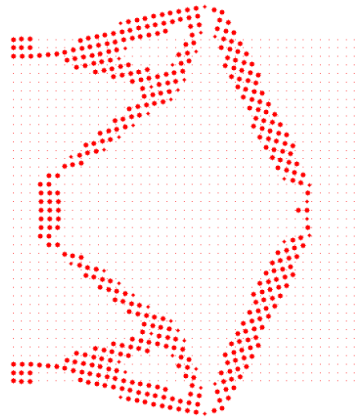
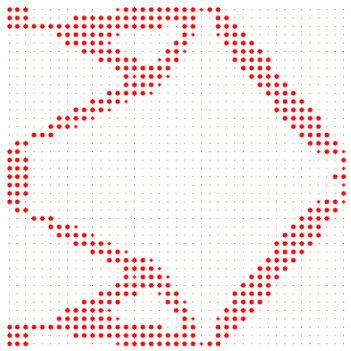


Linear modelling using EFG method

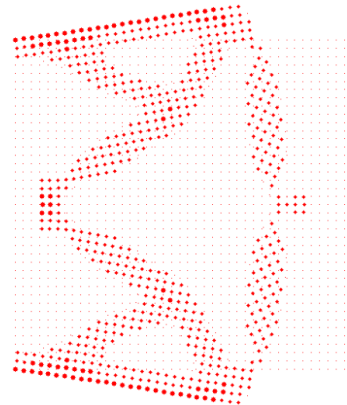
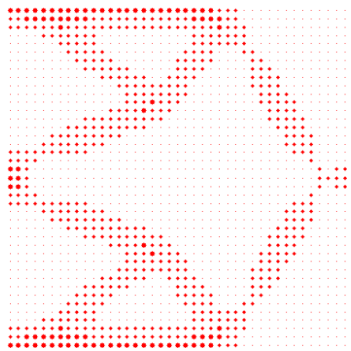


Non-linear modelling using FEM


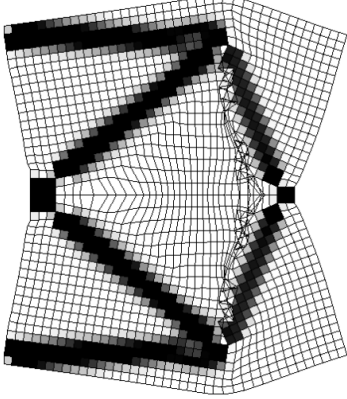
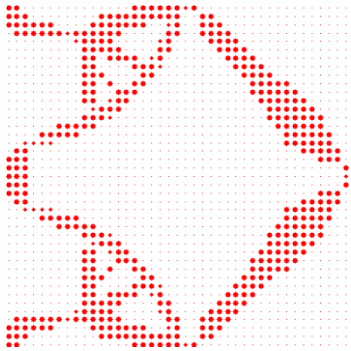
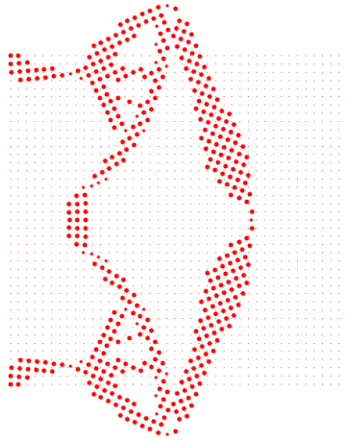
2



Non-linear modelling using EFG method



Linear modelling using EFG method

		
Non-linear modelling using FEM		
3		
Non-linear modelling using EFG method		

Furthermore, to show the advantage of the non-linear EFG method in the design compliant mechanism, the input force in Case 2 is enlarged to $F_{in}=1N$ in Case 3. During the numerical process, it is found that both the linear EFG model and non-linear FEM model experience convergent difficulty due to the output displacement is too large. For the linear EFG model, this problem may because of the limitation of the linear analysis. In regards to non-linear FEM analysis, this problem is due to the distortion of the element, which has reached the specified limitation. As to the proposed non-linear EFG method, however, this difficulty did not take place, in which the output displacement of optimal design can reach $122.8\mu m$. It is known that the displacement is a linear function of the applied load for the linear analysis, which means the loads of two cases are proportional and the resulting displacement fields are proportional as well. Hence, in linear analysis, two cases with proportional loads must result in the same optimized design. However, regarding to non-linear analysis, the resulting displacement is a non-linear function to the applied load, which will cause different optimal designs for two cases with proportional loads. Thus, it

can be seen that it is essential to use geometrically non-linear analysis in compliant mechanism design, and the proposed non-linear EFG method is more capable for large displacement problems.

7. Conclusions

This paper proposes an alternative topology optimization method for the design of large displacement compliant mechanisms with geometrical nonlinearity. The Shepard function method is applied to generate a non-local nodal density field with enriched smoothness over the design domain, so that there is no other filter scheme required during the numerical analysis. Furthermore, the Shepard function method is used again to interpolate the densities at all computational points. In this way, a physically meaningful material density representation is obtained based on a set of design variables located on the meshless field nodes. To implement the meshless approximations of state equations, the MLS method is used to construct shape functions with weight functions of compact support. The numerical example has demonstrated that the proposed method is capable to handle the design of large deformation compliant mechanism, and avoid the mesh distortion and convergent problem caused by large deformation. It is straightforward to extend the proposed topology optimization method to more advanced mechanics problems.

References

- [1] Allaire G., Jouve F., Toader A.M., Structural optimization using sensitivity analysis and a level-set method, *J Comput Phys*, 194 (2004) 363-393.
- [2] Atluri S.N., Zhu T., A new Meshless Local Petrov-Galerkin (MLPG) approach in computational mechanics, *Comput Mech*, 22 (1998) 117-127.
- [3] Atluri S.N., Shen S., The meshless local Petrov-Galerkin (MLPG) method, Crest, 2002.
- [4] Babuska I., Melenk J.M., The partition of unity finite element method, in, DTIC Document, 1995.
- [5] Bathe K.J., Finite element procedures, Prentice hall Englewood Cliffs, NJ, 1996.
- [6] Belytschko T., Lu Y.Y., Gu L., Element-free Galerkin methods, *Int J Numer Meth Eng*, 37 (1994) 229-256.
- [7] Belytschko T., Krongauz Y., Organ D., Fleming M., Krysl P., Meshless methods: an overview and recent developments, *Comput Methods Appl Mech Eng*, 139 (1996) 3-47.
- [8] Belytschko T., Moës N., Usui S., Parimi C., Arbitrary discontinuities in finite elements, *Int J Numer Meth Eng*, 50 (2001) 993-1013
- [9] Bendsøe M.P., Kikuchi N., Generating optimal topologies in structural design using a homogenization method, *Comput Methods Appl Mech Eng*, 71 (1988) 197-224.
- [10] Bendsøe M.P., Sigmund O., Material interpolation schemes in topology optimization, *Arch Appl Mech*, 69 (1999) 635-654.

- [11] Bendsøe M.P., Sigmund O., *Topology optimization: theory, methods and applications*, Springer, 2003.
- [12] Bourdin B., Filters in topology optimization, *Int J Numer Meth Eng*, 50 (2001) 2143-2158.
- [13] Bruns T.E., Sigmund O., Tortorelli D.A., Numerical methods for the topology optimization of structures that exhibit snapthrough, *Int J Numer Methods Eng*, 55(2002) 1215–1237.
- [14] Buhl T., Pedersen C.B.W., Sigmund O., Stiffness design of geometrically nonlinear structures using topology optimization, *Struct Multidiscip Optim*, 19(2000) 93-104.
- [15] Chen J.S., Pan C.H., Wu C.T., Liu W.K., Reproducing kernel particle methods for large deformation analysis of non-linear structures, *Comput Methods Appl Mech Eng*, 139 (1996) 195-227.
- [16] Du Y., Luo Z., Tian Q., Chen L., Topology optimization for thermo-mechanical compliant actuators using mesh-free methods, *Eng Optim*, 41 (2009) 753-772.
- [17] Duarte C.A., Oden J.T., An h-p adaptive method using clouds, *Comput Methods Appl Mech Eng*, 139 (1996) 237-262.
- [18] Gea H.C., Luo J.H., Topology optimization of structures with geometrical nonlinearities, *Comput Struct*, 79 (2001) 1977–1985.
- [19] Gingold R.A., Monaghan J.J., Smoothed particle hydrodynamics-theory and application to non-spherical stars, *Monthly notices of the royal astronomical society*, 181 (1977) 375-389.
- [20] Gu Y.T., Liu G.R., A boundary point interpolation method for stress analysis of solids, *Comput Mech*, 28 (2002) 47-54.
- [21] Guedes J.M., Kikuchi N., Preprocessing and postprocessing for materials based on the homogenization method with adaptive finite element methods, *Comput Methods Appl Mech Eng*, 83 (1990) 143-198.
- [22] Guest J.K., Prévost J.H., Belytschko T., Achieving minimum length scale in topology optimization using nodal design variables and projection functions, *Int J Numer Meth Eng*, 61 (2004) 238-254
- [23] He Q.Z., Kang Z., Wang Y.Q., A topology optimization framework for geometrically nonlinear structures with meshless analysis and independent density field interpolation, *Comput Mech*, 54 (2014) 629-644.
- [24] Howell L.L., *Compliant mechanisms*, John Wiley & Sons, 2001
- [25] Jog C., Distributed-parameter optimization and topology design for non-linear thermoelasticity, *Comput Methods Appl Mech Eng*, 132 (1996) 117–134.
- [26] Kang Z., Wang Y.Q., Structural topology optimization based on non-local Shepard interpolation of density field, *Comput Methods Appl Mech Eng*, 200 (2011) 3515-3525.
- [27] Kang Z., Wang Y.Q., A nodal variable method of structural topology optimization based on Shepard interpolant, *Int J Numer Meth Eng*, 90 (2011) 329–342.
- [28] Lekhnitskiĭ S.G., *Theory of elasticity of an anisotropic elastic body*, Holden-Day, 1963.
- [29] Liew K.M., Ren J., Reddy J.N., Numerical simulation of thermomechanical behaviours of shape memory alloys via a non-linear mesh-free Galerkin formulation, *Int J Numer Meth Eng*, 63 (2005) 1014-1040.
- [30] Liu G.R., Gu Y.T., A local radial point interpolation method (LRPIM) for free vibration analyses of 2-D solids, *J Sound Vib*, 246 (2001) 29-46.
- [31] Liu G.R., Gu Y.T., *An introduction to meshfree methods and their programming*, Springer, 2005.
- [32] Liu W.K., Jun S., Zhang Y.F., Reproducing kernel particle methods, *Int J Numer Meth Fl*, 20 (1995) 1081-1106.
- [33] Luo Z., Chen L., Yang J., Zhang Y., Abdel-Malek K., Compliant mechanism design using multi-objective topology optimization scheme of continuum structures, *Struct Multidiscip Optim*, 30 (2005) 142-154.

- [34] Luo Z., Tong L., Wang M.Y., Wang S., Shape and topology optimization of compliant mechanisms using a parameterization level set method, *J Comput Phys*, 227 (2007) 680-705.
- [35] Luo Z., Tong L., A level set method for shape and topology optimization of large-displacement compliant mechanisms, *Int J Numer Methods Eng*, 76 (2008) 862–892.
- [36] Luo Z., Zhang N., Gao W., Ma H., Structural shape and topology optimization using a meshless Galerkin level set method, *Int J Numer Methods Eng*, 90 (2012), 369-389.
- [37] Luo Z., Zhang N., Ji J., Wu T., A meshfree level-set method for topological shape optimization of compliant multiphysics actuators, *Comput Methods Appl Mech Eng*, 223 (2012) 133-152.
- [38] Luo Z., Zhang N., Wang Y., Gao W., Topology optimization of structures using meshless density variable approximants, *Int J Numer Methods Eng*, 93 (2013) 443-464.
- [39] Matsui K., Terada K., Continuous approximation of material distribution for topology optimization, *Int J Numer Meth Eng*, 59 (2004) 1925-1944.
- [40] Mlejnek H.P., Some aspects of the genesis of structures, *Struct Multidiscip Optim*, 5 (1992) 64-69.
- [41] Nocedal J., Wright S.J., Springer series in operations research. Numerical optimization, in, New York: Springer, 1999.
- [42] Paulino G.H., Le C.H., A modified Q4/Q4 element for topology optimization, *Struct Multidiscip Optim*, 37 (2009) 255-264.
- [43] Pedersen C.B.W., Buhl T., Sigmund O., Topology synthesis of large-displacement compliant mechanisms, *Int J Numer Meth Eng*, 50 (2001) 2683-2705.
- [44] Rahmatalla S.F., Swan C.C., A Q4/Q4 continuum structural topology optimization implementation, *Struct Multidiscip Optim*, 27 (2004) 130-135.
- [45] Sethian J.A., Wiegmann A., Structural boundary design via level set and immersed interface methods, *J Comput Phys*, 163 (2000) 489-528.
- [46] Sigmund O., Manufacturing tolerant topology optimization, *Acta Mechanica Sinica*, 25 (2009) 227-239.
- [47] Sigmund O., Design of multiphysics actuators using topology optimization-Part I: one-material structures, *Comput Methods Appl Mech Eng*, 190(2001) 6577–6604.
- [48] Sigmund O., Design of multiphysics actuators using topology optimization-Part II: two-material structures, *Comput Methods Appl Mech Eng*, 190 (2001) 6605–6627.
- [49] Wang M.Y., Wang X., Guo D., A level set method for structural topology optimization, *Comput Methods Appl Mech Eng*, 192 (2003) 227-246.
- [50] Wang Y., Luo Z., Zhang N., Topological Optimization of Structures Using a Multilevel Nodal Density-Based Approximant, *Comput Model Eng & Sci*, 84 (2012) 229-252.
- [51] Xie Y.M., Steven G.P., A simple evolutionary procedure for structural optimization, *Comput Struct*, 49 (1993) 885-896.
- [52] Yoon G.H., Kim Y.Y., Bendsøe M.P., Sigmund O., Hinge-free topology optimization with embedded translation-invariant differentiable wavelet shrinkage, *Struct Multidiscip Optim*, 27 (3) 139-150.
- [53] Zhou M., Rozvany G.I.N., The COC algorithm, Part II: topological, geometrical and generalized shape optimization, *Comput Method Appl M*, 89 (1991) 309-336.